Published in final edited form as:
J Med Chem. 2013 April 25; 56(8): 3429–3433. doi:10.1021/jm4001874.

Synthesis and Structure-Activity Relationships of 5,6,7-substituted Pyrazolopyrimidines: Discovery of a novel TSPO PET Ligand for Cancer Imaging

Dewei Tang[1,2], **Eliot T. McKinley**[1,3], **Matthew R. Hight**[1,4], **Md. Imam Uddin**[1,7], **Joel M. Harp**[5,6], **Allie Fu**[1], **Michael L. Nickels**[1,7], **Jason R. Buck**[1,7], and **H. Charles Manning**[1,2,3,7,8,9,*]

[1]Vanderbilt University Institute of Imaging Science (VUIIS), Vanderbilt University Medical Center, Nashville, TN

[2]Program in Chemical and Physical Biology, Vanderbilt University Medical Center, Nashville, TN

[3]Department of Biomedical Engineering, Vanderbilt University, Nashville, TN

[4]Interdisciplinary Materials Science Program, Department of Physics & Astronomy, Vanderbilt University, Nashville, TN

[5]Department of Biochemistry, Vanderbilt University Medical Center, Nashville, TN

[6]Department of Biological Sciences, Vanderbilt University, Nashville, TN

[7]Department of Radiology and Radiological Sciences, Vanderbilt University Medical Center, Nashville, TN

[8]Vanderbilt Ingram Cancer Center, Vanderbilt University Medical Center, Nashville, TN

[9]Department of Neurosurgery, Vanderbilt University Medical Center, Nashville, TN

Abstract

Focused library synthesis and structure-activity relationship development of 5,6,7-substituted pyrazolopyrimidines led to the discovery of 2-(5,7-diethyl-2-(4-(2-fluoroethoxy)phenyl)pyrazolo[1,5-*a*]pyrimidin-3-yl)-*N,N*-diethylacetamide (**6b**), a novel translocator protein (TSPO) ligand exhibiting a 36-fold enhancement in affinity compared to another pyrazolopyrimidine-based TSPO ligand, **6a** (DPA-714). Radiolabeling with fluorine-18 (^{18}F) facilitated production of 2-(5,7-diethyl-2-(4-(2-[^{18}F]fluoroethoxy)phenyl)pyrazolo[1,5-*a*]pyrimidin-3-yl)-*N,N*-diethylacetamide (**^{18}F-6b**) in high radiochemical yield and specific activity. *In vivo* studies of **^{18}F-6b** were performed which illuminated this agent as an improved probe for molecular imaging of TSPO-expressing cancers.

Introduction

There remains a critical need to develop and rigorously validate molecular imaging biomarkers that aid tumor diagnosis, predict clinical outcome, and quantify response to

*Corresponding Author: H. Charles Manning, Ph. D., Vanderbilt University Institute of Imaging Science (VUIIS), 1161 21st Ave. S., AA1105 MCN, Nashville, TN 37232-2310; Phone: 615-322-3793; Fax: 615-322-0734; henry.c.manning@vanderbilt.edu.

Author Contributions

Dr. Manning directed and designed the study. Mr. Tang performed the synthetic chemistry and along with Mr. McKinley, Mr. Hight, and Dr. Buck, performed the imaging experiments. Dr. Nickels performed the radiochemistry, Dr. Uddin and Dr. Harp carried out the crystallography. All authors participated in writing or editing the manuscript.

Supporting Information. Synthetic and analytical results for all compounds; Methods; Supplemental Figures. This material is available free of charge via the Internet at http://pubs.acs.org.

therapeutic interventions. Imaging techniques routinely used in clinical oncology include magnetic resonance imaging (MRI), X-ray computed tomography (CT), ultrasound imaging (US), and positron emission tomography (PET). Of these, the sensitivity and quantitative nature of PET, coupled with the ability to readily produce biologically active compounds bearing positron-emitting isotopes (e.g., ^{11}C, ^{18}F), renders PET imaging as one the most attractive techniques for detecting tumors and profiling their molecular features. By far, the most widely used PET tracer in clinical oncology is 2-deoxy-2-[^{18}F]fluoro-D-glucose (^{18}F-FDG), a probe that accumulates in tissue as a function of glucose utilization. PET using ^{18}F-FDG is a powerful approach for tumor detection in many organ sites. However, not all tumors exhibit elevated glucose avidity, and ^{18}F-FDG uptake can be affected by a plethora of normal metabolic processes. Furthermore, tumor imaging can be confounded by ^{18}F-FDG uptake in normal tissues such as healthy brain. These issues highlight an unmet need to explore and validate additional molecular targets for cancer imaging.

Our laboratory has explored translocator protein (TSPO) expression as a target for molecular imaging of cancer.[1–5] Formerly referred to as peripheral benzodiazepine receptor (PBR), TSPO is an 18-kDa protein typically localized to the outer mitochondria membrane. TSPO participates in the regulation of numerous cellular processes, including steroid biosynthesis, cholesterol metabolism, apoptosis, and cellular proliferation.[6] In normal tissues, TSPO tends to be expressed in those that produce steroids and those that are mitochondrial-enriched such as myocardium, skeletal muscle, and renal tissue. Tissues such as liver and brain exhibit comparatively modest expression.[6] While classically exploited as a target in neuroscience, elevated TSPO expression is also observed in many cancers.[13] In oncology, TSPO expression is typically linked with disease progression and diminished survival and is a hallmark of aggressive and potentially metastatic tumors.[13] For this reason, our laboratory has explored the use of TSPO imaging ligands within the context of colon cancer,[1] breast cancer, [2] and glioma,[4, 5] as these agents could potentially serve as useful cancer imaging biomarkers. We recently reported the first utilizations of the PET agents *N*-[^{18}F]fluoroacetyl-*N*-(2,5-dimethoxybenzyl)-2-phenoxyaniline (^{18}F-PBR06)[5] and *N,N*-diethyl-2-(2-(4-(2-[^{18}F]fluoroethoxy)phenyl)-5,7-dimethylpyrazolo[1,5-*a*]pyrimidin-3-yl)acetamide (^{18}F-DPA-714)[4] for quantitative assessment of TSPO expression in preclinical glioma. In these proof-of-principle PET imaging studies, tumors were detectable among surrounding normal brain and, importantly, TSPO levels could be quantitatively assayed in tumors using compartmental analysis of the PET data.[4, 5] However, drawbacks were observed with both agents in this context, including tracer accumulation in normal brain that reached levels potentially sufficient to prevent detection of gliomas with modest TSPO expression. Both tracers also exhibited significant metabolism *in vivo*, which required correction of plasma input functions for quantitative analysis. While illustrating the potential of TSPO PET to detect tumors in brain, these studies prompted our desire to develop novel TSPO PET ligands with improved properties for cancer imaging.

The goal of this study was to determine whether optimization of the pyrazolopyrimidine scaffold, specifically at the 5-, 6-, and 7-positions, would yield TSPO ligands with greater affinity and potentially serve as more robust PET imaging ligands *in vivo*. These experiments led to the discovery of 2-(5,7-diethyl-2-(4-(2-fluoroethoxy)phenyl)pyrazolo[1,5-*a*]pyrimidin-3-yl)-*N,N*-diethylacetamide (**6b**), a novel TSPO-selective ligand that exhibits a surprising 36-fold enhancement in affinity compared to another pyrazolopyrimidine, **6a** (DPA-714). An appropriate analog of **6b**, compound **7**, could be radiolabeled with fluorine-18 (^{18}F) to yield the novel TSPO PET ligand 2-(5,7-diethyl-2-(4-(2-[^{18}F]fluoroethoxy)phenyl)pyrazolo[1,5-*a*]pyrimidin-3-yl)-*N,N*-diethylacetamide (**^{18}F-6b**), which was subsequently evaluated *in vivo* in healthy rats and a preclinical model of glioma. **^{18}F-6b** exhibited negligible accumulation in normal brain, yet robust accumulation in tumor tissue, which facilitated excellent imaging contrast. Overall,

these studies illuminate **^{18}F-6b** as a promising, novel PET ligand for evaluating TSPO expression in tumors and potentially other diseases.

Results and Discussion

CHEMISTRY

MAOS of 5,6,7-substituted Pyrazolopyrimidine Library—A library of structurally diverse pyrazolopyrimidines (Table 1) was assembled using a microwave-assisted organic synthesis (MAOS) method that prioritized points of divergence at the 5-R_3, 6-R_2, and 7-R_1 positions on the core pyrazolopyrimidine scaffold. Members of this library were formed through condensation of a pyrazole core (**4**) with various substituted diones.[11] Entries in Table 1 fall into two distinct series (**5** and **6**), with seven compounds (**a**–**g**) per series. Each compound within the series results from one of seven diones utilized, while each series is differentiated by the installation of a unique surrogate imaging handle at the 4-postion (R_4) of the 2-phenyl group pendant to the core scaffold. Series 5 entries (**5a**–**5g**) feature a methoxy group at R_4 and include a previously reported pyrazolopyrimidine, **5a** (DPA-713),[7–10] while series 6 entries (**6a**–**6g**) feature a 2-fluoroethoxy group at R_4 and include **6a**.[7–9, 12] Given our ultimate goal of developing novel PET imaging ligands, coupled with an interest in expanding structure-activity relationships (SAR) around the 5,6,7-substituted pyrazolopyrimidine core, we rationalized that maintaining the surrogate imaging handles of future representative imaging probes would accelerate the development of novel agents.

The overall synthetic methodology is presented in Scheme 1.[11] Here, compound **4**, bearing a 3-amino-*1H*-pyrazole core, was accessible in two steps using MAOS from commercially available phenylpropanenitrile **1** and chloroacetamide **2**. From **4**, the synthesis diverges at the condensation step with a series of unique diones to yield the “five” series of pyrazolopyrimidines (**5a–5g**) that mimic analogous ^{11}C-based PET probes with an R_4-OMe. Subsequently, compounds **6a–6g** were achieved by cleavage of methoxy group followed by microwave–assisted ether synthesis with 2-fluoroethyl-4-methylbenzenesulfonate which yielded an R_4-2-fluoroethoxy surrogate imaging handle to mimic ^{18}F-labeled PET probes (Table 1). The library developed primarily explored the effects of R_1, R_2, and R_3 substituents that varied in steric bulk. Generally, substituents at R_1 and R_3 mirrored one another and consisted of linear and branched alkyl substituents such as methyl, ethyl, and isopropyl moieties. These substituents were cross-matched with similar groups at the R_2 position, which included hydrogen, methyl, ethyl, chloro, and 2-propanone.

Lipophilicity—Lipophilicity of series **5** and **6** were evaluated at pH = 7.5 (log $P_{7.5}$) using reversed phase HPLC[14] and is tabulated in Table 1. The values for library entries varied from 2.0 to 3.0 for both series and correlated predictably with dione structure, where polarity and hydrocarbon content of the R_1–R_3 substituents appeared to be key determinants. In both series, analogs a, d, and f, with R_1–R_3 combinations of hydrogen, methyl, and 2-propanone, proved the least lipophilic. Introduction of ethyl groups at R_1, R_2, or R_3 increased log $P_{7.5}$ values accordingly, as with analogs b and e, which ranged from 2.50–2.84. The most lipophilic analogs proved to be c and g (log $P_{7.5}$ = 2.55–2.99), with isopropyl groups at the R_1 and R_3 positions or chlorine at R_2. Interestingly, of the two series, series **5** (R_4 = OMe), tended to be more lipophilic than series **6** (R_4 = OCH_2CH_2F). Overall, the library entries exhibited lipophilicities (2.07–2.99) suitable for *in vivo* imaging,[15] where potential agents must be sufficiently membrane penetrant to bind intracellular targets such as TSPO.

BIOLOGICAL TESTING

Binding Affinity in Cancer Cell Lysate and SAR Analysis—To evaluate binding of the library entries to TSPO, radioligand displacement was carried out in rat glioma cell lysate (C6) using *N*-(sec-butyl)-1-(2-chlorophenyl)-*N*-methyl-^{3}H-isoquinoline-3-carboxamide (^{3}H-PK 11195)[4, 5]. Affinities of library members are expressed as *K*i (nM) values in Table 1. Encompassing modifications at R_1–R_4, both series exhibited a spectrum of *K*i values that spanned micromolar to sub-nanomolar affinity. As expected, replacing the 4-methoxy with 4-(2-fluoroethoxy) at the R_4 position had minimal impact upon TSPO affinity, as similar SAR trends emerged within series 5 and 6. In contrast, R_1, R_2, and R_3 modification led to major impacts upon affinity. Though the R_1 and R_3 positions showed intolerance to steric bulk beyond ethyl, a surprising level of improvement in affinity could be realized by replacing methyl with ethyl at the R_1 and R_3 positions. For example, subnanomolar affinities (*K*i) were observed for analogs **5b** (0.18 nM) and **6b** (0.27 nM), which represent major improvements over their respective leads, **5a** (12.23 nM) and **6a** (9.73 nM) (Table 1), as well as another high-affinity TSPO ligand, *N*-(2-methoxybenzyl)-*N*-(4-phenoxypyridin-3-yl)acetamide (PBR28) (4.0 nM)[16]. Increasing the R_1 and R_3 to a bulkier isopropyl group proved detrimental, with *K*i values for both **5c** and **6c** greater than 500 nM. Overall, the R_2 position was less tolerant to steric or electron density deviations from hydrogen in these studies. Substitution of the nascent R_2 hydrogen (**5a**, **6a**) with methyl (**5d**, 93.75 nM; **6d**, 83.04 nM) decreased affinity approximately 10-fold with respect to their parent compounds, **5a** and **6b**, respectively; this trend was more dramatic with ethyl substitution (**5e**, 157.14 nM; **6e**, 276.79 nM). Introduction of polarity at the R_2 position with 2-propanone (**5f**, 200.89 nM; **6f**, 251.79 nM) bore similar adverse effects upon affinity. Somewhat less dramatic decreases in affinity were observed upon halogen substitution at R_2 with chlorine (**5g**, 55.36 nM; **6g**, 67.86 nM). Given the size of chlorine atom, lying between methyl and ethyl, it is reasonable that the *K*i of entries **5g** and **6g** are only slightly worse than those with alkyl substituents at the R_2 position (Table 1). Overall, these experiments illuminated 5,7-diethyl, 6-hydrogen substitution as the optimal pattern in this series to impart improved affinity. Additionally, the studies also suggested that an analog could be produced for PET imaging using either fluorine-18 (**6b**) or carbon-11 (**5a**) substitution on the R_4 position with minimal effect on TSPO affinity and only minor effect on lipophilicity. Since fluorine-18 has a significantly longer half-life than carbon-11 (109.8 min vs. 20.4 min), we elected to carry compound **6b** forward for further characterization. The selectivity of compound **6b** for TSPO over the central benzodiazepine receptor (CBR) was evaluated using radioligand displacement of the CBR ligand ^{3}H-flunitrazepam in rat cerebral cortex membranes (Table 1). Unlike the displacement studies with ^{3}H-PK 11195, compound **6b** demonstrated poor affinity for CBR (*K*i > 10,000 nM), indicating TSPO selectivity.

RADIOCHEMISTRY

Radioligand Precursor Preparation and Radiosynthesis—To produce **^{18}F-6b**, we synthesized precursor (**7**), a tosylated intermediate prepared from **5b** in two steps with an overall yield of approximately 45% (Scheme 1). Nucleophilic fluorination of **7** with fluorine-18 was then performed (Scheme 1) in anhydrous dimethyl sulfoxide at 165 °C for 5 minutes. Purification of **^{18}F-6b** was carried out with preparative HPLC using 10 mM sodium phosphate buffer (pH 6.7) in ethanol (47.5/52.5, v/v). The retention time of **^{18}F-6b** was 12 minutes according to gamma detection and corresponded to the UV retention time of non-radioactive **6b**. Radiochemical purity was consistently greater than 99%, with specific activity consistently greater than 4203 Ci/mmol (156 TBq/mmol) (n = 33).

IMAGING STUDIES

Uptake of ^{18}F-6b in C6 Glioma—The *in vivo* performance of **^{18}F-6b** was evaluated in glioma-bearing Wistar rats using microPET imaging, with a typical study shown in Figure 1. MRI (T_2-weighted) was used to localize tumors and for registration of anatomical features with PET[4, 5] (Figure 1A). Dynamic PET imaging with **^{18}F-6b** illustrated that the majority of tracer uptake in the brain was localized to the tumor, with very modest accumulation in the adjacent, normal brain (Figure 1B and 1C). The tumor-selective uptake characteristics of **^{18}F-6b** afforded excellent imaging contrast between tumor and normal tissue. In addition to the tumor, accumulation of **^{18}F-6b** was observed outside of the brain in olfactory epithelium and the Harderian glands, as well as the tongue, where TSPO expression is elevated.[13] Figure 1D illustrates time-activity curves (TACs) that were typical of eight representative studies for tumor, normal brain, and plasma over a 90-minute dynamic acquisition. We found that **^{18}F-6b** was rapidly delivered to tumor and normal brain, but cleared tumor tissues at a much slower rate than normal brain. After an initial spike in radioactivity consistent with tracer injection and rapid distribution, **^{18}F-6b** quickly cleared from the plasma. To validate the PET, imaging-matched brains were processed for *post mortem* staining and immunohistochemistry. We observed close agreement between tumor tissue (H&E, Figure 1E), elevated TSPO expression by immunohistochemistry (Figure 1F), and tumor accumulation of **^{18}F-6b** accumulation (Figure 1C). To more quantitatively compare the performance of **^{18}F-6b** to **^{18}F-6a**, we conducted dynamic PET using **^{18}F-6b** in a cohort of tumor-bearing rats (n = 5) and carried out pharmacokinetic modeling of the PET data, similar to our previous studies[4, 5]. We found that **^{18}F-6b** demonstrated a higher ratio of total distribution volume (V_T) between tumor and normal brain (6.0, n = 5), when compared to **^{18}F-6a** (3.9, n =11),[4] which resulted in greater signal-to-noise between tumor and surround normal brain.

Characterization of ^{18}F-6b Radiometabolites in Plasma—Analogous to our previous work,[4] radio-HPLC was used to evaluate metabolism of **^{18}F-6b** in plasma at multiple time points during the PET scanning period (2, 12, 30, 60, 90 min) (Supplemental Figure 1). Parent compound (**^{18}F-6b**) was the only radioactive species detected in plasma at all time points, suggesting a lack of circulating **^{18}F-6b** metabolites observed over a 90-minute period. This behavior contrasted the *in vivo* performance of **^{18}F-6a**, where we previously observed up to 30% metabolism within the first 12 minutes post-administration.[4] Potentially, the apparent improved stability of **^{18}F-6b** over **^{18}F-6a** may stem from the rapid clearance of **^{18}F-6b** from plasma, rendering detection of low levels of metabolites challenging with HPLC.

Biodistribution and Specific Binding of ^{18}F-6b in Rats—The biodistribution and TSPO-specificity of **^{18}F-6b** was evaluated in normal tissues. Tissue samples were harvested 60 minutes after infusion of the **^{18}F-6b**. The radioactivity of harvested tissue was measured using standard analytical methods and recorded as percentage of the injected dose per gram of tissue (%ID/g) (Supplemental Figure 2A). Consistent with known TSPO densities,[13] we observed elevated accumulation of **^{18}F-6b** in spleen, heart, kidney, and lung.[17] Moderate uptake was also observed in liver, colon, small bowel, and stomach. Very minor accumulation was observed in the brain, testes, skull, and skeletal muscle. At 60 minutes post-administration of tracer, very little radio-activity was observed in biological fluids, such as whole blood or urine.

To evaluate the specific binding of **^{18}F-6b** in normal tissue, we carried out a similar 60-minute biodistribution assay that included a bolus infusion of non-radioactive **6b** (10 mg/kg) at 30 minutes (Supplemental Figure 2B). With displacement, we observed that activity in the organs exhibiting the greatest accumulation of **^{18}F-6b**, such as spleen, heart, kidney, and

lung, was reduced to background levels, indicating near complete displacement and reversible binding in healthy tissue. Organs that exhibited low to moderate accumulation of **^{18}F-6b** without displacement, such as muscle or liver, were essentially unchanged with displacement, suggesting that the low to moderate tracer accumulation in these tissues may reflect non-specificity. Interestingly, activity found in the urine did not follow this trend and was elevated with displacement, suggesting that blocking TSPO with non-radioactive **6b** altered the excretion profile of the agent. Overall, the results indicate a high degree of specific binding and reversibility of **^{18}F-6b** to TSPO in healthy tissues.

CRYSTALLOGRAPHY

6b was recrystallized from hot acetonitrile and ethanol (95%) by slow evaporation at room temperature and characterized by diffractometry. **6b** demonstrated two ethyl branches at the 5- and 7-positions of the pyrazolopyrimidine ring, corresponding to the structure elucidated from NMR spectroscopy. The crystal structure also revealed three distinct planar entities, the pyrazolopyrimidine ring, the phenyl ring, and the amide group (Supplemental Figure 3).

Conclusion

In this study, we found that the 5,6,7-substitution pattern is a critical determinant of TSPO affinity among pyrazolopyrimidines. Experiments shown here led to the discovery of **6b**, a TSPO ligand exhibiting significantly increased affinity compared to **6a** and TSPO ligands derived from other chemical entities.[18] Furthermore, in addition to improved TSPO affinity, compound **6b** was TSPO-selective, exhibiting negligible binding affinity to CBR. Analog **7** of **6b** could be radiolabeled with fluorine-18 to yield **^{18}F-6b**. Suggesting its potential as a probe for cancer imaging, preclinical imaging studies demonstrated robust accumulation of **^{18}F-6b** in tumor tissue and negligible accumulation in normal brain. Overall, these studies illuminate **^{18}F-6b** as a promising, novel PET ligand for evaluating TSPO expression in tumors and potentially other diseases.

Supplementary Material

Refer to Web version on PubMed Central for supplementary material.

Acknowledgments

Funding Sources

The authors acknowledge funding from the National Institutes of Health (K25 CA127349, P50 CA128323, S10 RR17858, U24 CA126588, 1R01 CA163806), The Kleberg Foundation, and The Lustgarten Foundation.

M. Noor Tantawy, George H. Wilson, Dan Colvin and Yiu-Yin Cheung are acknowledged.

References

1. Deane NG, Manning HC, Foutch AC, Washington MK, Aronow BJ, Bornhop DJ, Coffey RJ. Targeted imaging of colonic tumors in smad3−/− mice discriminates cancer and inflammation. Mol Cancer Res. 2007; 5:341–349. [PubMed: 17426249]
2. Wyatt SK, Manning HC, Bai M, Bailey SN, Gallant P, Ma G, McIntosh L, Bornhop DJ. Molecular imaging of the translocator protein (TSPO) in a pre-clinical model of breast cancer. Mol Imaging Biol. 2010; 12:349–358. [PubMed: 19949989]
3. Manning HC, Goebel T, Thompson RC, Price RR, Lee H, Bornhop DJ. Targeted molecular imaging agents for cellular-scale bimodal imaging. Bioconjug Chem. 2004; 15:1488–1495. [PubMed: 15546219]

4. Tang D, Hight MR, McKinley ET, Fu A, Buck JR, Smith RA, Tantawy MN, Peterson TE, Colvin DC, Ansari MS, Nickels M, Manning HC. Quantitative preclinical imaging of TSPO expression in glioma using N,N-diethyl-2-(2-(4-(2-18F-fluoroethoxy) phenyl)-5,7-dimethylpyrazolo[1,5-a]pyrimi din-3-yl)acetamide. J Nucl Med. 2012; 53:287–294. [PubMed: 22251555]
5. Buck JR, McKinley ET, Hight MR, Fu A, Tang D, Smith RA, Tantawy MN, Peterson TE, Colvin D, Ansari MS, Baldwin RM, Zhao P, Guleryuz S, Manning HC. Quantitative, preclinical PET of translocator protein expression in glioma using ^{18}F-N-fluoroacetyl-N-(2,5-dimethoxybenzyl)-2-phenoxyaniline. J Nucl Med. 2011; 52:107–114. [PubMed: 21149488]
6. Papadopoulos V, Baraldi M, Guilarte TR, Knudsen TB, Lacapere JJ, Lindemann P, Norenberg MD, Nutt D, Weizman A, Zhang MR, Gavish M. Translocator protein (18kDa): new nomenclature for the peripheral-type benzodiazepine receptor based on its structure and molecular function. Trends Pharmacol Sci. 2006; 27:402–409. [PubMed: 16822554]
7. Chauveau F, Van Camp N, Dolle F, Kuhnast B, Hinnen F, Damont A, Boutin H, James M, Kassiou M, Tavitian B. Comparative evaluation of the translocator protein radioligands ^{11}C-DPA-713, ^{18}F-DPA-714, and ^{11}C-PK11195 in a rat model of acute neuroinflammation. J Nucl Med. 2009; 50:468–476. [PubMed: 19223401]
8. Doorduin J, Klein HC, Dierckx RA, James M, Kassiou M, de Vries EF. [^{11}C]-DPA-713 [^{18}F]-DPA-714 as new PET tracers for TSPO: a comparison with [^{11}C]-(R)-PK11195 in a rat model of herpes encephalitis. Mol Imaging Biol. 2009; 11:386–398. [PubMed: 19330384]
9. James ML, Fulton RR, Henderson DJ, Eberl S, Meikle SR, Thomson S, Allan RD, Dolle F, Fulham MJ, Kassiou M. Synthesis and in vivo evaluation of a novel peripheral benzodiazepine receptor PET radioligand. Bioorg Med Chem. 2005; 13:6188–6194. [PubMed: 16039131]
10. Selleri S, Bruni F, Costagli C, Costanzo A, Guerrini G, Ciciani G, Costa B, Martini C. 2-Arylpyrazolo[1,5-a]pyrimidin-3-yl acetamides. New potent and selective peripheral benzodiazepine receptor ligands. Bioorg Med Chem. 2001; 9:2661–2671. [PubMed: 11557354]
11. Tang D, Buck JR, Hight MR, Manning HC. Microwave-assisted Organic Synthesis of a High-affinity Pyrazolo-pyrimidinyl TSPO Ligand. Tetrahedron Lett. 2010; 51:4595–4598. [PubMed: 20689673]
12. Martin A, Boisgard R, Theze B, Van Camp N, Kuhnast B, Damont A, Kassiou M, Dolle F, Tavitian B. Evaluation of the PBR/TSPO radioligand [(18)F]DPA-714 in a rat model of focal cerebral ischemia. J Cereb Blood Flow Metab. 2010; 30:230–241. [PubMed: 19794397]
13. Batarseh A, Papadopoulos V. Regulation of translocator protein 18 kDa (TSPO) expression in health and disease states. Mol Cell Endocrinol. 2010; 327:1–12. [PubMed: 20600583]
14. Waterhouse RN, Mardon K, Giles KM, Collier TL, O'Brien JC. Halogenated 4-(phenoxymethyl)piperidines as potential radiolabeled probes for sigma-1 receptors: in vivo evaluation of [^{123}I]-1-(iodopropen-2-yl)-4-[(4-cyanophenoxy)methyl]pip eri dine. J Med Chem. 1997; 40:1657–1667. [PubMed: 9171875]
15. Pike VW. PET radiotracers: crossing the blood-brain barrier and surviving metabolism. Trends Pharmacol Sci. 2009; 30:431–440. [PubMed: 19616318]
16. Owen DR, Howell OW, Tang SP, Wells LA, Bennacef I, Bergstrom M, Gunn RN, Rabiner EA, Wilkins MR, Reynolds R, Matthews PM, Parker CA. Two binding sites for [^{3}H]PBR28 in human brain: implications for TSPO PET imaging of neuroinflammation. J Cereb Blood Flow Metab. 2010; 30:1608–1618. [PubMed: 20424634]
17. Fujimura Y, Kimura Y, Simeon FG, Dickstein LP, Pike VW, Innis RB, Fujita M. Biodistribution and radiation dosimetry in humans of a new PET ligand, (18)F-PBR06, to image translocator protein (18 kDa). J Nucl Med. 2010; 51:145–149. [PubMed: 20008980]
18. Taliani S, Pugliesi I, Da Settimo F. Structural requirements to obtain highly potent and selective 18 kDa Translocator Protein (TSPO) Ligands. Curr Top Med Chem. 2011; 11(7):860–886. [PubMed: 21291396]

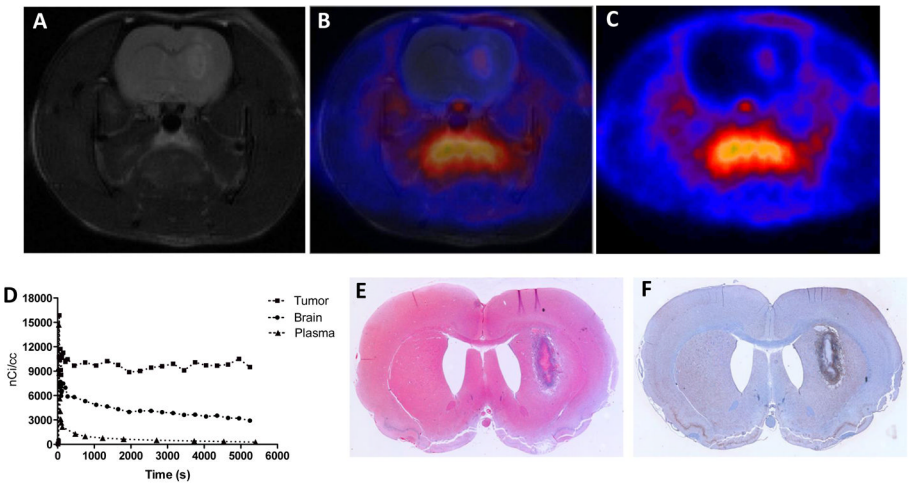

Figure 1.
PET imaging of preclinical glioma using **^{18}F-6b.**

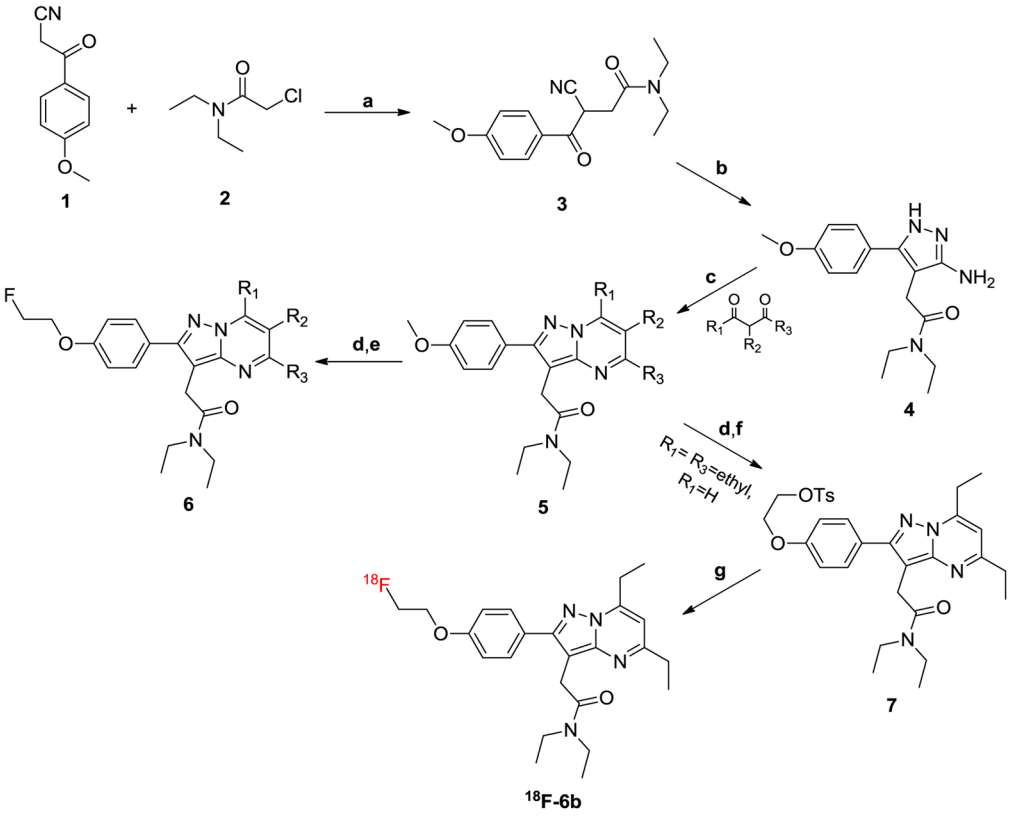

Scheme 1. Synthetic methodology utilized to generate a focused library of 5,6,7-substituted pyrazolopyrimidines and ^{18}F-6b[α]

[α]Reagents and conditions: (a) NaOH, NaI, microwave, 80 °C, 40 min, 80% EtOH in H_2O, 70%; (b) hydrazine, AcOH, microwave, 90 °C, 40 min, EtOH, 42%; (c) microwave, 140–190 °C, 45min, EtOH, 10–90%; (d) HTPB, microwave, 110 °C, 40 min, aqueous HBr; (e) NaH, 2-fluoroethyl-4-methylbenzenesulfonate, microwave, 120 °C, 30 min, dry THF. (f) ethylene di(*p*-toluenesulfonate), NaH, microwave, 120 °C, 30 min, dry THF, 45%. (g) Fluoride-18 ion, K^+-$K_{2.2.2}$/K_2CO_3, 99 °C, 20 min, dry DMSO.

J Med Chem. Author manuscript; available in PMC 2014 April 25.

Table 1

Affinity, liphopilicity, and molecular weight of pyraxolopyrimidines

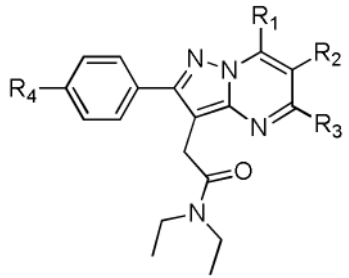

Compd	R_1	R_2	R_3	R_4	MW	$LogP_{7.5}$	*Ki* (nM)[δ]
5a[α]	-Me	-H	-Me	-OMe	366.21	2.40	12.23
5b	-Et	-H	-Et	-OMe	394.51	2.84	0.18
5c[β]	-iPr	-H	-iPr	-OMe	422.56	2.98	>500
5d	-Me	-Me	-Me	-OMe	380.48	2.45	93.75
5e	-Me	-Et	-Me	-OMe	394.51	2.78	157.14
5f	-Me	$-CH_2C(O)CH_3$	-Me	-OMe	408.49	2.57	200.89
5g	-Me	-Cl	-Me	-OMe	400.9	2.99	55.36
6a[γ]	-Me	-H	-Me	$-OCH_2CH_2F$	398.47	2.12	9.73
6b	-Et	-H	-Et	$-OCH_2CH_2F$	426.53	2.50	0.27[ε]
6c	-iPr	-H	-iPr	$-OCH_2CH_2F$	454.58	2.73	>500
6d	-Me	-Me	-Me	$-OCH_2CH_2F$	412.5	2.47	83.04
6e	-Me	-Et	-Me	$-OCH_2CH_2F$	426.53	2.53	276.79
6f	-Me	$-CH_2C(O)CH_3$	-Me	$-OCH_2CH_2F$	440.51	2.07	251.79
6g	-Me	-Cl	-Me	$-OCH_2CH_2F$	432.92	2.55	67.86

[α] DPA-713, see references.[7–10]

[β] See reference.[11]

[γ] DPA-714, see references.[7–9, 12]

[δ] Competitive binding against ^{3}H-PK 11195 in C6 glioma cell lysate.

[ε] K_i *versus* ^{3}H-flunitrazepam > 10,000 nM.